CrystEngComm

Accepted Manuscript

ROYAL SOCIETY OF CHEMISTRY

www.rsc.org/crystengcomm

Cite this: DOI: 10.1039/c0xx00000x

www.rsc.org/xxxxxx

ARTICLE TYPE

A series of coordination polymers tuned terphenyl tetracarboxylates and bis-pyridyl ligands with different flexibilities manifesting fluorescence properties and photocatalytic activities

Bao Mu, Ru-Dan Huang*

Key Laboratory of Cluster Science of Ministry of Education, School of Chemistry, Beijing Institute of Technology, Beijing, 100081, P. R. China

Received (in XXX, XXX) Xth XXXXXXXXX 200X, Accepted Xth XXXXXXXXX 200X
DOI: 10.1039/b000000x

A family of new two-dimensional (2D) and three-dimensional (3D) coordination polymers, namely, $[Co(\mathbf{H_2L})(\mathbf{bpe})_2]_n$ (**1**), $[Co_2(\mathbf{L})(\mathbf{bpmp})(H_2O)]_n$ (**2**), $[Co(\mathbf{H_2L})(\mathbf{bpfp})(H_2O)_2]_n$ (**3**), $\{[Ni(\mathbf{H_2L})(\mathbf{bpe})(H_2O)_2]\cdot 2H_2O\}_n$ (**4**), $[Ni(\mathbf{L})_{0.5}(\mathbf{bpmp})_{0.5}]_n$ (**5**), $\{[Cd(\mathbf{H_2L})(\mathbf{bpe})_{0.5}(H_2O)_2]\cdot 0.5(\mathbf{bpe})\}_n$ (**6**) and $\{[Cd_2(\mathbf{L})(\mathbf{bpfp})_{0.5}]\cdot H_2O\}_n$ (**7**) were constructed using the [1,1′:4′,1″-terphenyl]-2′,4,4″,5′-tetracarboxylic acid ($\mathbf{H_4L}$), the transition metals and the bis-pyridyl ligands (**bpe** = 1,2-bi(pyridin-4-yl)ethene, **bpmp** = N,N′-bis(4-pyridyl)piperazine and **bpfp** = bis(4-pyridylformyl)piperazine) with different flexibilities. These complexes were characterized by elemental analyses, IR spectra, thermogravimetric (TG) analyses, powder X-ray diffraction (PXRD) and single-crystal X-ray diffraction. Complex **1** represents a 2D coordinate layer consisted of the metal Co^{II} ions and $\mathbf{H_2L}$ ligands, and the monodentate bpe ligands hang both sides of the network. Complex **2** is a (4, 6)-connected 3D framework based on Co-**L** 2D sheets with four kinds of different quadrilaterals and the bridging **bpmp** ligands. When **bpmp** is replaced by **bpfp**, complex **3** possesses a 2D (4, 4) network containing the "H"-type 1D Co-$\mathbf{H_2L}$ chains and 1D Co-**bpfp** zigzag chains. Complex **4** is similar with complex **3** except for containing the 1D Ni-**bpe** straight chains. Complex **5** displays a 3D framework with the symmetrical polygonal windows, in which there are the 2D grids composed by the same size of quadrilaterals. Complex **6** exhibits a 2D $\{6^3\}$ layer including hexagonal grids, and some non-coordinated bpe ligands exist in the network. When **bpfp** is used in complex **7**, a 3D complicated $\{4^{15}\cdot 6^{13}\}_2\{4^2\cdot 6^3\cdot 8\}\{4^7\cdot 6^3\}_4$ framework is formed. In this structure, all the coordinated atoms from the **L** and **bpfp** ligands coordinate with the metal Cd^{II} ions. Furthermore, the 2D layers of complexes **1**, **3**, **4** and **6** are ultimately expanded to 3D supramolecular frameworks through the hydrogen bonding interactions. The flexibility of the bis-pyridyl ligands indicates consequential influence on the final architectures of complexes **1**–**7**. Moreover, the electrochemical behaviors and the fluorescence properties have been investigated. Photocatalytic properties reveal that complex **3** represents good catalytic activities for the degradation of organic dye methylene blue (MB).

Introduction

Enormous scientific research has been dedicated to the exploration of coordination polymers for the past few years, which is ascribed to not only the miscellaneous architectures and absorbing topologies, but also the desirable applications such as gas adsorption/separation, magnetism, fluorescence, ion exchange and catalysis [1]. In the field of catalysis, in particular, photocatalysis as a kind of ecological technology can efficaciously abate toxic organic dyes from industrial wastewater, which has very promising future in the environmental field [2]. Except that the conventional semiconductor metal oxides can be usually regarded as photocatalysts, plenty of coordination polymers possessing good photocatalytic efficiency have got much attention [3]. In some coordination polymers, different interactions between inorganic moieties and organic moieties may give rise to the different metal−organic ligand charge transfer in the tunable photocatalysts [4]. Up till the present moment, some research groups apply themselves to studying the

Key Laboratory of Cluster Science of Ministry of Education, School of Chemistry, Beijing Institute of Technology, Beijing, 100081, P. R. China; Email: huangrd@bit.edu.cn

†Electronic Supplementary Information (ESI) available: IR, TG and additional figures. CCDC:1426939−1426945. For ESI and crystallographic data in CIF or other electronic format see DOI: 10.1039/b000000x.

photocatalytic properties of metal-organic coordination polymers, and they have made some progress [5]. For example, Wang et al. utilize organic bis-pyridyl-bis-amide ligands and various carboxylates to synthesize a series of Cu^{II} and Co^{II} coordination polymers, and the photocatalytic results reveal that some coordination polymers may be the photocatalytic materials on account of their wonderful catalytic activities for the degradation of methylene blue (MB) [5a-b]. Ma et al. obtained a heterotrimetallic organic coordination polymer, which displays the high and stable photocatalytic activity toward 4-chlorophenol at pH 3 through the comparison of different pH values [5e]. In view of the excellently degradative effect, it is worth exploring new photocatalytic materials bearing the remarkable photocatalytic properties further.

On the other hand, the reasonable strategies are significant for constructing architectures with special properties [6]. In the course of design, lots of influential factors, such as the reaction time and temperature, the molar ratio of reactants, synthetic method, should be taken into account because they are closely bound up the final constructions [7]. The organic ligands, as one of the most crucial factors, are divided into many varieties [8]. Thereinto, typical multifunctional O-donor polycarboxylates ligands are the excellent candidates, which is beneficial to the self-assembly of coordination polymers [9]. Especially, the rigid tetracarboxylates ligands based on terphenyl moieties recently become a focus of attention [10-11]. So far, this kind of ligands has been introduced into the coordination polymers to construct some high dimensional frameworks and coordination framework materials with application properties, such as the great luminescent properties, higher H_2 storage capacity, which not only is due to the presence of the delocalized π-electron system, but also is because the rigid terphenyl moieties are in favor of generating the pore framework [10f, 11c]. Moreover, these tetracarboxylates ligands can provide the charge producing the ·OH active species from excited state to oxygenate water molecules, which may generate the photocatalytic effect for degradation some organic dyes. In this contribution, we choose terphenyl tetracarboxylates [1,1′:4′,1″-terphenyl]-2′,4,4″,5′-tetracarboxylic acid (**H_4L**) as the main ligand and three types of N-donor bis-pyridyl ligands 1,2-bi(pyridin-4-yl)ethane (**bpe**), N,N′-bis(4-pyridyl)piperazine (**bpmp**) and bis(4-pyridylformyl)piperazine) (**bpfp**) as the secondary ligands, and report the preparation and structural features of a series of coordination polymers based on the transition metal ions (Co^{II}, Ni^{II} and Cd^{II}), formulas, $[Co(\mathbf{H_2L})(\mathbf{bpe})_2]_n$ (**1**), $[Co_2(\mathbf{L})(\mathbf{bpmp})(H_2O)]_n$ (**2**), $[Co(\mathbf{H_2L})(\mathbf{bpfp})(H_2O)_2]_n$ (**3**), $\{[Ni(\mathbf{H_2L})(\mathbf{bpe})(H_2O)_2]\cdot 2H_2O\}_n$ (**4**), $[Ni(\mathbf{L})_{0.5}(\mathbf{bpmp})_{0.5}]_n$ (**5**), $\{[Cd(\mathbf{H_2L})(\mathbf{bpe})_{0.5}(H_2O)_2]\cdot 0.5(\mathbf{bpe})\}_n$ (**6**) and $\{[Cd_2(\mathbf{L})(\mathbf{bpfp})_{0.5}]\cdot H_2O\}_n$ (**7**). The electrochemical behaviors of complexes **1**–**5** as well as the fluorescence properties of the title complexes have been examined. In addition, the photocatalytic properties present that the title complexes display different degradative effects for organic dye MB.

Experimental section

Materials and characterization

All the chemicals were obtained from the commercial sources without further purification. The elemental analyses (C, H, and N) were performed on a Perkin-Elmer 2400 CHN elemental analyzer. The FT-IR spectra (KBr pellets) were recorded on a Nicolet 170SX spectrometer. The powder X-ray diffraction (PXRD) were taken on a Siemens D5005 diffractometer (Cu Ka radiation, λ = 1.5410 Å). Thermogravimetric (TG) analyses of the title complexes were taken on a Exstar SII TG/DTA 7200 thermal analyzer. Fluorescence spectra were collected using a Hitachi F-4600 fluorescence/phosphorescence spectrophotometer. UV-Vis absorption spectra were carried out on a TU-1901 UV-vis spectrophotometer. Photocatalytic experiment was measured on a PLS-LAX500 apparatus. Electrochemical measurements were measured on a CHI 660E Electrochemical Quartz Crystal Microbalance. The complex bulk-modified carbon paste electrode (CPE), Ag/AgCl and the platinum wire was used as the working electrode, reference electrode and auxiliary electrode, respectively.

Preparation of the title complexes

Synthesis of $[Co(H_2L)(bpe)_2]_n$ (1) The mixture of $Co(NO_3)_2\cdot 6H_2O$ (0.0582 g, 0.20 mmol), **H_4L** (0.0406 g, 0.10 mmol), **bpe** (0.0364 g, 0.20 mmol), NaOH (0.004 g, 0.10 mmol) and H_2O (10 mL) was placed in a 25 mL Teflon reaction kettle, and it was kept at 150°C for 3 days. When the reaction kettle was cooled to room temperature, the red block crystals were collected. Yield 28% based on Co. Anal. Calc. for $C_{46}H_{32}CoN_4O_8$ (827.69): C, 66.75; H, 3.90; N, 6.77%. Found: C, 66.79; H, 3.87; N, 6.75%. IR (KBr, cm^{-1}): 3132 (s), 2778 (w), 2609 (w), 2498 (w), 2361 (w), 1901 (w), 1699 (m), 1604 (m), 1565 (m), 1401 (s), 1275 (m), 1120 (w), 1067 (w), 1016 (m), 957 (w), 911 (w), 864 (m), 833 (s), 795 (m), 778 (m), 709 (w), 671 (w), 552 (s).

Table 1 Crystal data and structure refinement for complexes 1–7

Complex	1	2	3	4	5	6	7
Formula	$C_{46}H_{32}CoN_4O_8$	$C_{38}H_{32}Co_2N_4O_9$	$C_{38}H_{32}CoN_4O_{12}$	$C_{34}H_{30}NiN_2O_{12}$	$C_{19}H_{15}NiN_2O_4$	$C_{34}H_{26}CdN_2O_{10}$	$C_{30}H_{20}Cd_2N_2O_{10}$
Formula wt	827.69	806.54	795.61	717.29	394.01	734.98	793.30
Cryst. syst	Triclinic	Triclinic	Triclinic	Triclinic	Triclinic	Triclinic	Monoclinic
Space group	*P-1*	*P-1*	*P-1*	*P-1*	*P -1*	*P -1*	*P2(1)/c*
a (Å)	9.7060(8)	9.2805(7)	6.6150(5)	9.3587(7)	8.9520(7)	8.0510(8)	11.1050(11)
b (Å)	9.8389(9)	10.7128(8)	10.2951(9)	9.7400(8)	10.1019(9)	10.0389(9)	19.2931(16)
c (Å)	20.4971(18)	17.9162(15)	14.1409(12)	10.5441(9)	10.887(2)	18.4301(15)	15.0216(11)

α (°)	91.899(1)	103.410(2)	111.300(2)	68.7810(10)	90.8700(10)	87.918(2)	90
β (°)	92.021(1)	102.141(2)	92.6190(10)	64.0200(10)	104.2800(10)	79.934(1)	125.643(5)
γ (°)	109.147(2)	94.2650(10)	96.1730(10)	88.873(2)	111.042(2)	87.256(2)	90
V (Å ^{3})	1845.9(3)	1679.6(2)	888.30(13)	794.29(11)	884.6(2)	1464.2(2)	2615.5(4)
Z	2	2	1	1	2	2	4
D_{calc} (g/cm^3)	1.489	1.595	1.487	1.500	1.479	1.667	2.015
μ/mm^{-1}	0.531	1.054	0.556	0.681	1.123	0.813	1.695
F(000)	854	828	411	372	406	744	1560
R_{int}	0.0395	0.0461	0.0442	0.0459	0.0949	0.1021	0.1961
R_1[a] [$I>2\sigma(I)$]	0.0472	0.0523	0.0531	0.0509	0.0862	0.0983	0.0810
wR_2[b](all data)	0.0853	0.0839	0.1368	0.1034	0.1906	0.2766	0.1776
GOF	0.989	0.984	0.999	1.046	0.996	1.079	1.028
$\Delta\rho_{max}$(e Å^{-3})	0.849	0.638	0.811	0.648	0.736	4.710	2.115
$\Delta\rho_{min}$(e Å^{-3})	–0.678	–0.431	–0.587	–0.551	–0.602	–2.208	–2.779

[a] $R_1 = \Sigma(||F_o| - |F_c||)/\Sigma|F_o|$ [b] $wR_2 = [\Sigma w(|F_o|^2 - |F_c|^2)^2/(\Sigma w|F_o|^2)^2]^{1/2}$

Table 2. Coordination modes of H_4L ligand in complexes 1−7. Color legend: pink, Co; green, Ni; yellow, Cd; light gray, C; red, O; charcoal gray, H.

Complex 1	Complex 2	Complex 3	Complex 4	Complex 5	Complex 6	Complex 7
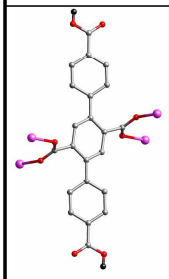	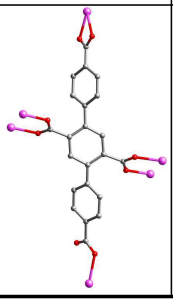	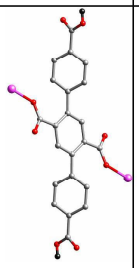	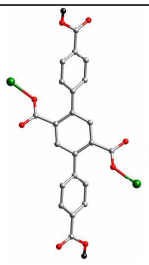	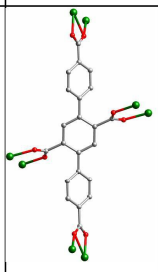	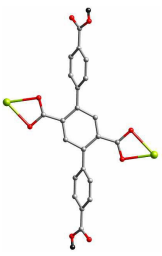	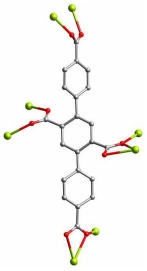

Synthesis of $[Co_2(L)(bpmp)(H_2O)]_n$ (2) The synthetic procedure of **2** was similar to that of **1** except for using **bpmp** (0.0536 g, 0.20 mmol) replace **bpe**, and the red crystals were obtained. Yield 23% based on Co. Anal. Calc. for $C_{38}H_{32}Co_2N_4O_9$ (806.54): C, 56.59; H, 4.00; N, 6.95%. Found: C, 56.62; H, 3.97; N, 6.99%. IR (KBr, cm^{-1}): 3132 (s), 2810 (w), 2355 (w), 1594 (s), 1506 (s), 1401 (s), 1155 (m), 1135 (m), 1057 (m), 1013 (s), 927 (m), 870 (s), 827 (m), 802 (m), 778 (s), 739 (m), 710 (s), 671 (m), 627 (w), 621 (m), 587 (s), 521 (m).

Synthesis of $[Co(H_2L)(bpfp)(H_2O)_2]_n$ (3) The synthetic conditions of **3** were the same as **1** except for using **bpfp** (0.0592 g, 0.20 mmol) instead of **bpe** to get red crystals. Yield 31% based on Co. Anal. Calc. for $C_{38}H_{32}CoN_4O_{12}$ (795.61): C, 57.37; H, 4.05; N, 7.04%. Found: C, 57.32; H, 4.01; N, 7.08%. IR (KBr, cm^{-1}): 3122 (s), 2997 (w), 2667 (w), 2560 (w), 2355 (w), 1950 (w), 1849 (w), 1682 (s), 1644 (s), 1606 (s), 1562 (s), 1462 (m), 1401 (s), 1338 (m), 1282 (m), 1183 (m), 1126 (w), 1101 (w), 1064 (m), 1001 (s), 963 (w), 927 (w), 896 (w), 852 (s), 789 (s), 770 (m), 720 (s), 640 (m), 596 (m), 533 (m).

Synthesis of $\{[Ni(H_2L)(bpe)(H_2O)_2]\cdot 2H_2O\}_n$ (4) The mixture of $Ni(NO_3)_2\cdot 6H_2O$ (0.1746 g, 0.60 mmol), **H_4L** (0.0203 g, 0.05 mmol), **bpe** (0.0091 g, 0.05 mmol), 1 mol·L^{-1} HCl aqueous solution (0.13 mL) and H_2O (10 mL) was transfered in a 25 mL Teflon reaction kettle, and it was heated at 160°C for 3 days. Green block crystals were collected. Yield 6% based on Ni. Anal. Calc. for $C_{34}H_{30}NiN_2O_{12}$ (717.29): C, 56.93; H, 4.22; N, 3.91%. Found: C, 56.96; H, 4.19; N, 3.96%. IR (KBr, cm^{-1}): 3133 (s), 2997 (w), 2642 (w), 2528 (w), 2367 (m), 1925 (w), 1837 (w), 1689 (s), 1609 (s), 1550 (s), 1401 (s), 1344 (m), 1282 (m), 1183 (m), 1120 (m), 1076 (w), 1039 (w), 1020 (s), 988 (s), 927 (m), 858 (s), 827 (s), 808 (s), 764 (s), 720 (s), 665 (w), 590 (m), 546 (m), 516 (w).

Synthesis of $[Ni(L)_{0.5}(bpmp)_{0.5}]_n$ (5) The mixture of $Ni(NO_3)_2\cdot 6H_2O$ (0.0871 g, 0.30 mmol), **H_4L** (0.0203 g, 0.05 mmol), **bpmp** (0.0268 g, 0.10 mmol), NaOH (0.006 g, 0.15 mmol) and H_2O (7.5 mL) was put in a 25 mL Teflon reaction kettle, and heated at 210°C for 3 days. The green crystals were obtained. Yield 8% based on Ni. Anal. Calc. for $C_{19}H_{15}NiN_2O_4$ (394.01): C, 57.92; H, 3.84; N, 7.11%. Found: C, 57.96; H, 3.82; N, 7.13%. IR (KBr, cm^{-1}): 3127 (s), 2810 (w), 2361 (w), 1603 (s), 1484 (w), 1398 (s), 1357 (m), 1288 (w), 1263 (w), 1219 (w), 1142 (m), 1064 (w), 1010 (m), 908 (w), 858 (m), 795 (m), 770 (s), 745 (m), 715 (m), 677 (m), 615 (w), 577 (m), 516 (m).

Synthesis of $\{[Cd(H_2L)(bpe)_{0.5}(H_2O)_2]\cdot 0.5(bpe)\}_n$ (6) A mixture of $CdCl_2\cdot 2.5H_2O$ (0.0456 g, 0.20 mmol), **H_4L** (0.0406 g, 0.10

mmol), **bpe** (0.0364 g, 0.20 mmol), NaOH (0.006 g, 0.15 mmol) and H_2O (10 mL) was placed in a 25 mL Teflon reactor, keeping at 150°C for 3 days. Cooling to room temperature, the yellow block crystals were isolated. Yield 10% based on Cd. Anal. Calcd for $C_{34}H_{26}CdN_2O_{10}$ (734.98): C, 55.56; H, 3.57; N, 3.81%. Found: C, 55.59; H, 3.54; N, 3.82%. IR (KBr, cm^{-1}): 3146 (s), 1942 (w), 1674 (s), 1600 (s), 1565 (s), 1494 (m), 1388 (s), 1291 (m), 1200 (m), 1126 (w), 1076 (m), 1045 (w), 1007 (s), 988 (s), 864 (s), 833 (s), 778 (s), 715 (m), 665 (w), 615 (w), 596 (m), 546 (s).

Synthesis of $\{[Cd_2(L)(bpfp)_{0.5}]\cdot H_2O\}_n$ (7) The synthetic step of **7** is similar with that of **6** except that **bpfp** (0.0592 g, 0.20 mmol) substitute for **bpe**. The yellow crystals were obtained. Yield 13% based on Cd. Anal. Calcd for $C_{30}H_{20}Cd_2N_2O_{10}$ (793.30): C, 45.42; H, 2.54; N, 3.53%. Found: C, 45.47; H, 2.52; N, 3.51%. IR (KBr, cm-1): 3122 (s), 1942 (w), 1569 (s), 1401 (s), 1275 (s), 1257 (s), 1219 (m), 1170 (w), 1139 (m), 1101 (m), 1064 (m), 996 (s), 938 (m), 893 (w), 864 (s), 778 (s), 739 (s), 709 (m), 665 (m), 583 (m), 516 (m).

Preparation of complexes 1–5 bulk-modified carbon paste electrode

The **1**–CPE was prepared as follows: the mixture of 0.032 g complex **1** and 0.5 g graphite powder were ground through agate mortar and pestle for 30 min. About 0.18 mL paraffin oil was added into the mixture with stirring uniformly, which was used to pack 3 mm inner diameter glass tubes with 0.8 cm length. The electrical contact was built with the copper stick, and the surface of the **1**–CPE was polished on the weighing paper. The other CPEs were made with complexes **2**–**5** by the similar method.

X-ray crystallographic study

Single-crystal X-ray diffraction data for the title complexes were collected on a Bruker APEX diffractometer with Mo Kα (graphite monochromator, λ=0.71073 Å) at 298 K. The structures of complexes **1**–**7** were solved through direct methods and refined through the full-matrix least-squares methods on F^2 with the SHELXTL package [12a], and complexes **1**, **3** and **4** were also solved through Olex2 1.2 software [12b-c]. All the non-hydrogen atoms were refined anisotropically and the hydrogen atoms of the organic ligands were generated theoretically. The crystallographic data and structure refinement parameters of complexes **1**–**7** are summarized in **Table 1**. Selected bond distances (Å) and angles (o) for complexes **1**–**7** are listed in **Tables S1**−**S7** (Supporting Information). The hydrogen-bonding parameters for the part of complexes are summarized in **Tables S8**−**S11**. The CCDC numbers 1426939−1426945 for complexes **1**−**7** are the supplementary crystallographic data in this paper, which can be obtained free of charge via www.ccdc.cam.ac.uk/conts/retrieving.html.

Results and discussion

Description of crystal structures

$[Co(H_2L)(bpe)_2]_n$ (1)

The structural analysis exhibits that complex **1** is a 3D supramolecular framework containing the 2D Co-H_2L coordination layers. Complex **1** crystallizes triclinic P-1 space group, and the asymmetric unit is composed of two crystallographically independent Co^{II} ions each lying on independent inversion centres, two half H_2L ligands each lying about other independent inversion centres and two **bpe** ligands. Both Co1 and Co2 are lighted by four carboxylic oxygen atoms

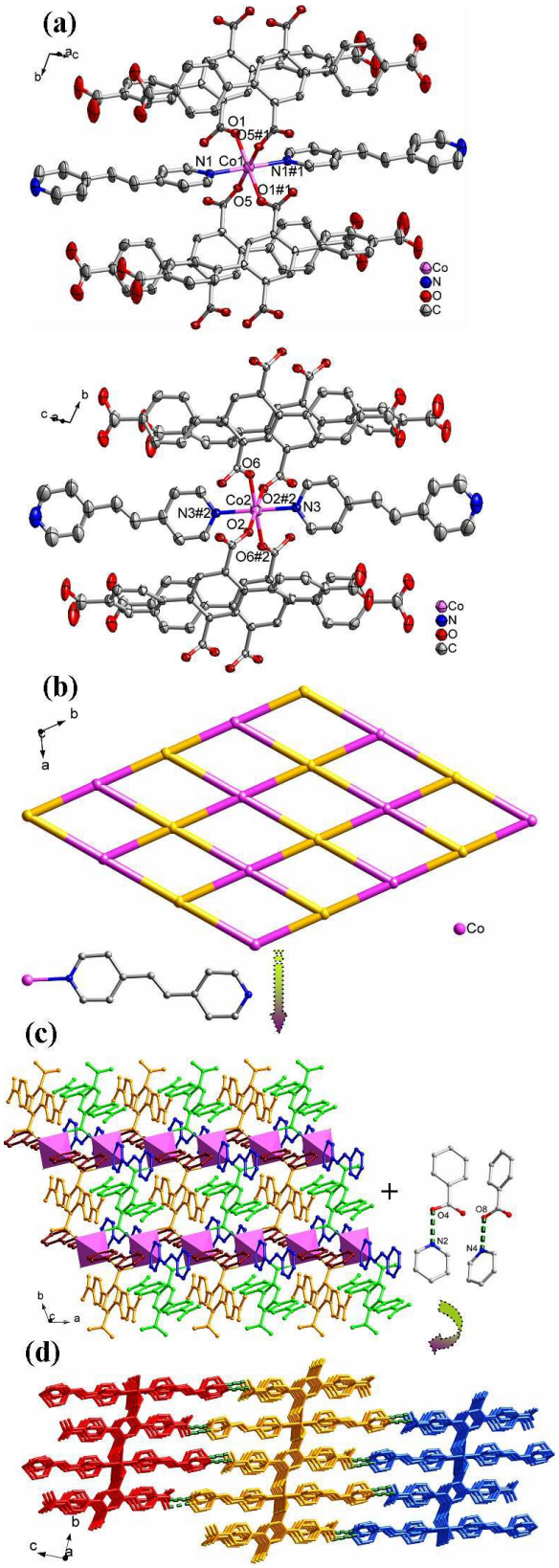

Fig. 1. (a) The coordination environment of the Co^{II} ion in complex **1** (#1 – *x*, 1 – *y*, – *z*; #2 1 – *x*, 1 – *y*, – *z*). (b) The schematic of 2D layer of **1**. (c)

The 2D structure of **1**. (d) View of 3D supramolecular framework formed by hydrogen-bonding interactions in **1**.

from four separate $\mathbf{H_2L}$ ligands and two pyridine nitrogen atoms from two separate **bpe** ligands, adopting the distorted $\{CoO_4N_2\}$ octahedral coordination geometries (**Fig. 1a**). The distances of Co–O and Co–N are in the range of 2.054(3)–2.099(3) Å and 2.157(4)–2.189(4) Å, respectively. $\mathbf{H_2L}$ ligand of complex **1** as a partially deprotonated ligand presents μ_2-η^1:η^1 (bidentate) coordination pattern (**Table 2**), and they possess two kinds of dihedral angles between two-sided parallel phenyl rings and the central phenyl ring. The dihedral angles are 37.82º and 24.60º, respectively. The μ_4-bridging $\mathbf{H_2L}$ ligands are linked by Co^{II} ions to produce a 4-connected 2D coordination layer with the Schläfli symbol of $\{4^4\cdot6^2\}$ (**Fig. 1b**), in which the Co-O A-chains and $\mathbf{H_2L}$ ligands arrange alternately, and the neighboring $\mathbf{H_2L}$ ligands display different twist angles (**Fig. S1**).

The **bpe** ligand shows the monodentate coordination mode, and they possess two different dihedral angles (7.13º and 10.72º) between two pyridine rings, hanging both sides of 2D structure (**Fig. 1c**). The adjacent 2D layers are further extended to yield a 3D supramolecular framework through the protonated carboxylate oxygen atoms (O4, O8) from $\mathbf{H_2L}$ ligands and the non-coordinated nitrogen atoms (N2, N4) from **bpe** ligands with the O4–H4···N2 and O8–H8···N4 distances of 2.6382 Å and 2.7427 Å, respectively (**Fig. 1d**).

$[Co_2(\mathbf{L})(\mathbf{bpmp})(H_2O)]_n$ (2)

Compared with complex **1**, the N-donor ligand **bpe** was replaced by the **bpmp** ligand, and a 3D coordination polymer based on metal Co^{II} ions, the N-donor **bpmp** ligands and the **L** carboxylic ligands was obtained. It crystallizes triclinic system with P-1 space group as well. There are two crystallographically independent Co^{II} ions, one **L** ligand, one **bpmp** ligand and one coordinated water molecule in the asymmetric unit. Although both Co1 and Co2 locate the distorted $\{CoO_4N\}$ square-pyramidal coordination configuration, they show different coordination environment (**Fig. 2a**). Co1 is occupied by four carboxylic oxygen atoms (O1, O5#1, O6#4, O7#4) of three separate **L** ligands and one nitrogen atom (N1) of **bpmp** ligand. The distances of Co1–O and Co1–N are 1.985(3)–2.200(3) Å and 2.058(3) Å, respectively. Co2 is surrounded by three carboxylic oxygen atoms (O2, O4#1, O8#3) of four separate **L** ligands, one nitrogen atom (N4#2) of **bpmp** ligand and one coordinated water molecule (O3). The distances of Co2–O and Co2–N are 2.002(3)–2.206(3) Å and 2.100(4) Å, respectively. The fully deprotonated **L** ligand takes on three kinds of coordination patterns (**Table 2**). Both carboxylic groups of central phenyl ring are coordinated with two metal Co^{II} ions, respectively, exhibiting the μ_2-η^1:η^1 bidentate coordination mode. The carboxylic groups of two-sided phenyl rings display the μ_1-η^1:η^0 and μ_1-η^1:η^1 coordination mode, respectively. The dihedral angle between two-sided phenyl rings is 13.08º, and they have the dihedral angles of 45.70º and 41.12º with the central phenyl ring, respectively. Seven carboxylic oxygen atoms from four μ_6-bridging **L** ligands link Co^{II} ions to construct a dinuclear Co^{II} unit with the Co···Co distance of 3.18 Å, which are connected by the **L** ligands to generate a 2D structure containing quadrilaterals with four kinds of different sizes of 9.22 Å × 11.95 Å, 12.44 Å × 9.08 Å, 12.18 Å × 8.99 Å and 12.47 Å × 8.81 Å, respectively. The slight distinction may be due to difference in dihedral angles between the central phenyl ring and two-sided phenyl rings (**Fig. 2b and Fig. S2**). The μ_2-bridging N-donor **bpmp** ligands with dihedral angles of 20.02º between two pyridine rings link the neighbouring 2D structures to give a 3D architecture (**Fig. 2c and Fig. S3**).

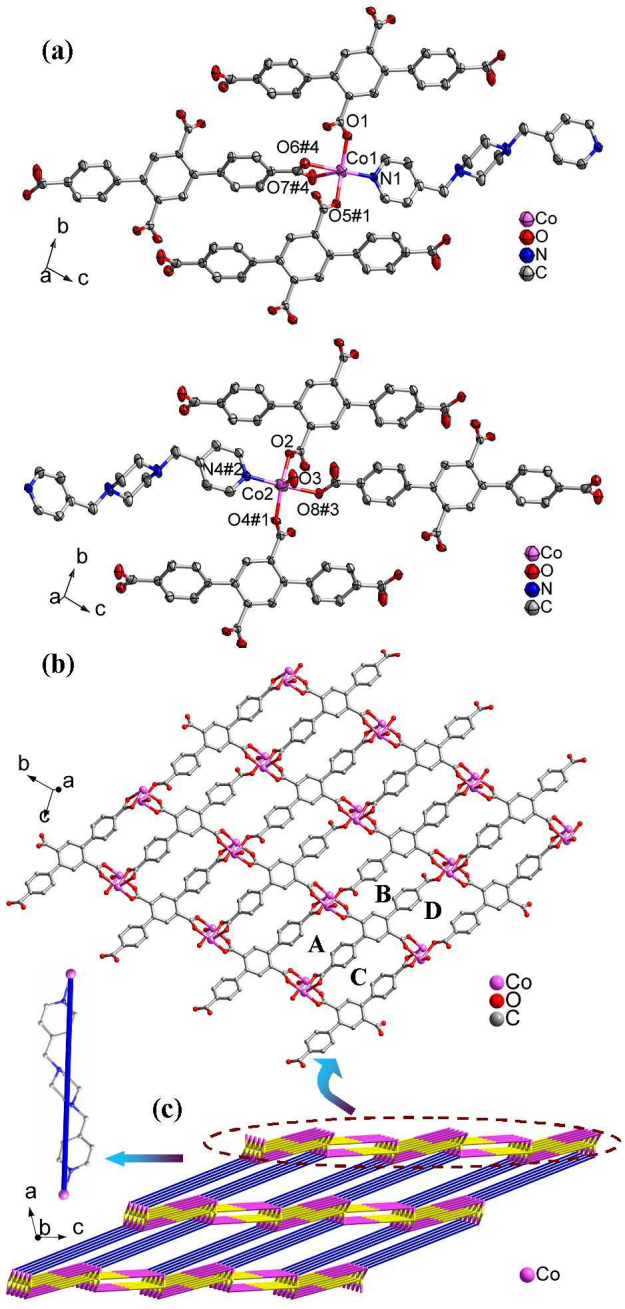

Fig. 2. (a) The coordination environment of the Co^{II} ion in complex **2** (#1 x, $1+y$, z; #2 $1+x$, $1+y$, $1+z$; #3 $1-x$, $-y$, $1-z$; #4 $1-x$, $1-y$, $2-z$). (b) The 2D network including four kinds of quadrilaterals with different sizes. (c) The schematic of the (4,6)-connected 3D framework with $\{4^3\cdot6^3\}_2\{4^6\cdot6^6\cdot8^3\}$ topology.

From topological viewpoint, Co1 and Co2 ions are both coordinated by three **L** ligands and one **bpmp** ligand, respectively, which are considered as 4-connected nodes. The **L** ligand linking three Co1 and three Co2 ions, which is considered as a 6-

connected node, and the **bpmp** ligand as a linker connects two metal Co^{II} ions. The final structure can be simplified as (4, 6)-connected $\{4^3\cdot6^3\}_2\{4^6\cdot6^6\cdot8^3\}$ framework (**Fig. 2c**).

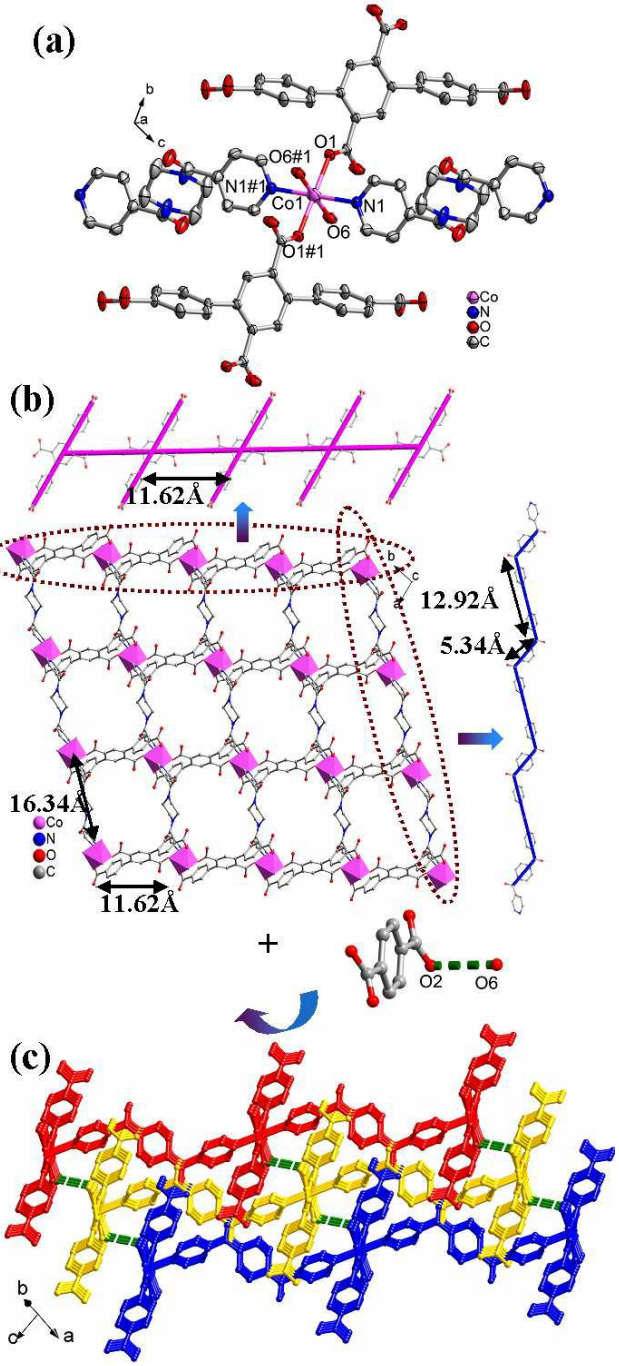

Fig. 3. (a) The coordination environment of the Co^{II} ion in complex **3** (#1 $1-x, 1-y, 1-z$). (b) The 2D grid with two kinds of 1D chains in **3**. (c) View of 3D supramolecular framework formed by hydrogen-bonding interactions in **3**.

*[Co(**H_2L**)(**bpfp**)$(H_2O)_2]_n$ (3)*

When the **bpmp** ligand was instead of **bpfp** ligand, a 3D supramolecular framework containing (4,4)-connected grids was obtained. The X-ray crystal data reveals that complex **3** also belongs to triclinic system with space group of P-1. The asymmetric unit is made up of one crystallographically independent Co^{II} ion lying on an inversion centre, one half of an **H_2L** ligand lying about another independent inversion centre, a half **bpfp** ligand lying about another inversion centre and two coordinated water molecules. Each central Co^{II} ion is in a distorted

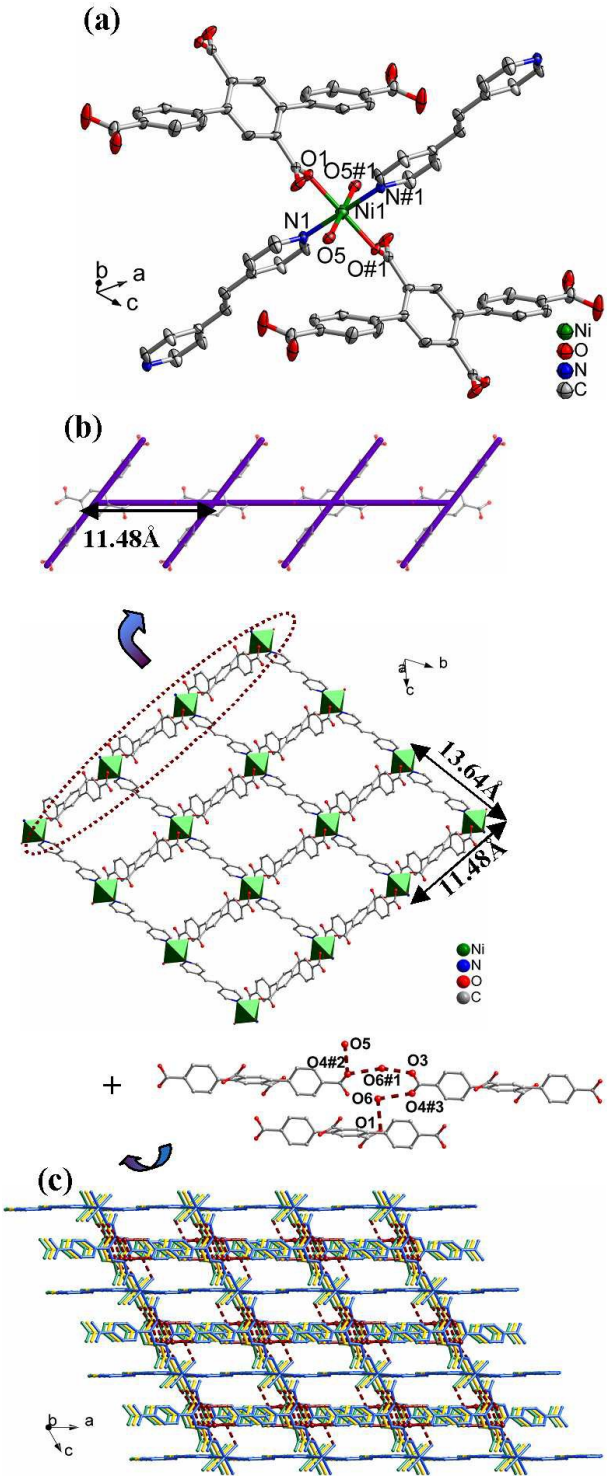

Fig. 4. (a) The coordination environment of the Ni^{II} ion in complex **4** (#1 $1-x, 1-y, 1-z$). (b) The 2D layer of **4** (#1 $1+x, y, z$; #2 $-1+x, y, 1+z$; #3 $2-x, 1-y, -z$). (c) View of 3D supramolecular framework formed by hydrogen-bonding interactions in **4**.

$\{CoO_4N_2\}$ coordination environment, which is environed by two oxygen atoms (O1, O1#1) of two separate **H_2L** ligands, two

oxygen atoms (O6, O6#1) of two coordinated water molecules and two pyridine nitrogen atoms (N1, N1#1) of two separate **bpfp** ligands (**Fig. 3a**). The distances of Co–O and Co–N are in the range of 2.094(2)–2.096(2) Å and 2.159(3) Å, respectively. The μ_1-η^1:η^0 monodentate **H_2L** ligands bridge the metal Co^{II} ions to form a "H"-type 1D chain with the intersection point separation of 11.62 Å, and two parallel phenyl rings have the dihedral angle of 61.43° with the central phenyl ring. The **bpfp** ligands with the parallel pyridine rings are connected by the Co^{II} ions to yield a non-symmetrical 1D zigzag chain with the distances of 11.62 Å and 16.34 Å from the neighbouring inflection point. Two kinds of 1D chains combine each other, giving rise to a (4, 4) 2D grid with the dimension of 11.62 × 16.34 $Å^2$ (**Fig. 3b**).

The 2D grids are sustained through the O–H···O hydrogen bonding interactions between the coordinated water molecules (O6) and the non-coordinated oxygen atoms (O2) from the **H_2L** ligands, generating a 3D supramolecular framework. The distance of O6–H6C···O2 hydrogen bond is 2.8565 Å (**Fig. 3c**).

*{[Ni(**H_2L**)(**bpe**)$(H_2O)_2$]·$2H_2O$}$_n$ (**4**)*

The space group of complex **4** is the same as that of the above complexes, and complex **4** is a 3D supramolecular framework based on the 2D grid sheets. The asymmetric unit includes one crystallographically independent Ni^{II} ion lying on an inversion centre, a half **H_2L** ligand lying about another inversion centre, one half of a **bpe** ligand lying about another independent inversion centre, two coordinated water molecules and two lattice water molecules. The centre Ni^{II} ion is bonded by two oxygen atoms (O1, O1#1) of two separate **H_2L** ligands, two oxygen atoms (O5, O#1) of two coordinated water molecules and two pyridine nitrogen atoms (N1, N1#1) of two separate **bpe** ligands, displaying the distorted $\{NiO_4N_2\}$ octahedral coordination configuration (**Fig. 4a**). The distances of Ni–O and Ni–N are 2.0621(19)–2.087(2) Å and 2.122(3) Å, respectively. Compared with **H_2L** ligand in complex **1**, the carboxylates from two-sided parallel phenyl rings in **H_2L** ligand of complex **4** are protonated, but both carboxylic groups from the central phenyl ring take on μ_1-η^1:η^0 monodentate coordination mode (**Table 2**). The dihedral angle between the two-sided phenyl rings and the central phenyl ring is 51.72°. The μ_2-bridging **H_2L** ligands are connected by the metal Ni^{II} ions to form a "H"-type 1D chain with the intersection point separation of 11.48 Å, and two nitrogen atoms of bis-pyridine **bpe** ligands link the metal Ni^{II} ions to form the 1D straight chain (**Fig. S4**). Two kinds of 1D chains combine, resulting in a 4-connected 2D grid with the Schläfli symbol of $\{4^4\cdot6^2\}$, and the dimension is about 11.48 × 13.64 $Å^2$, which is smaller than that in complex **3** (**Fig. 4b and Fig. S5**).

The 2D grids are further extended to produce a 3D supramolecular framework by two kinds of O–H···O hydrogen bonding interactions (**Fig. 4c**). One is formed between the coordinated water molecules and the carboxylic oxygen atoms with the O5–H5B···O4 distance of 2.8645 Å. The other is formed between the lattice water molecules and the carboxylic oxygen atoms with the O3–H3···O6, O6–H6A···O1 and O6–H6B···O4 distances of 2.5775 Å, 2.7637 Å and 2.8654 Å, respectively.

*[Ni(**L**)$_{0.5}$(**bpmp**)$_{0.5}$]$_n$ (**5**)*

The structural analysis exhibits that complex 5 features a (5,8)-connected 3D metal-organic framework consisting of the 2D metal-carboxylate coordination layers, and it belongs to triclinic

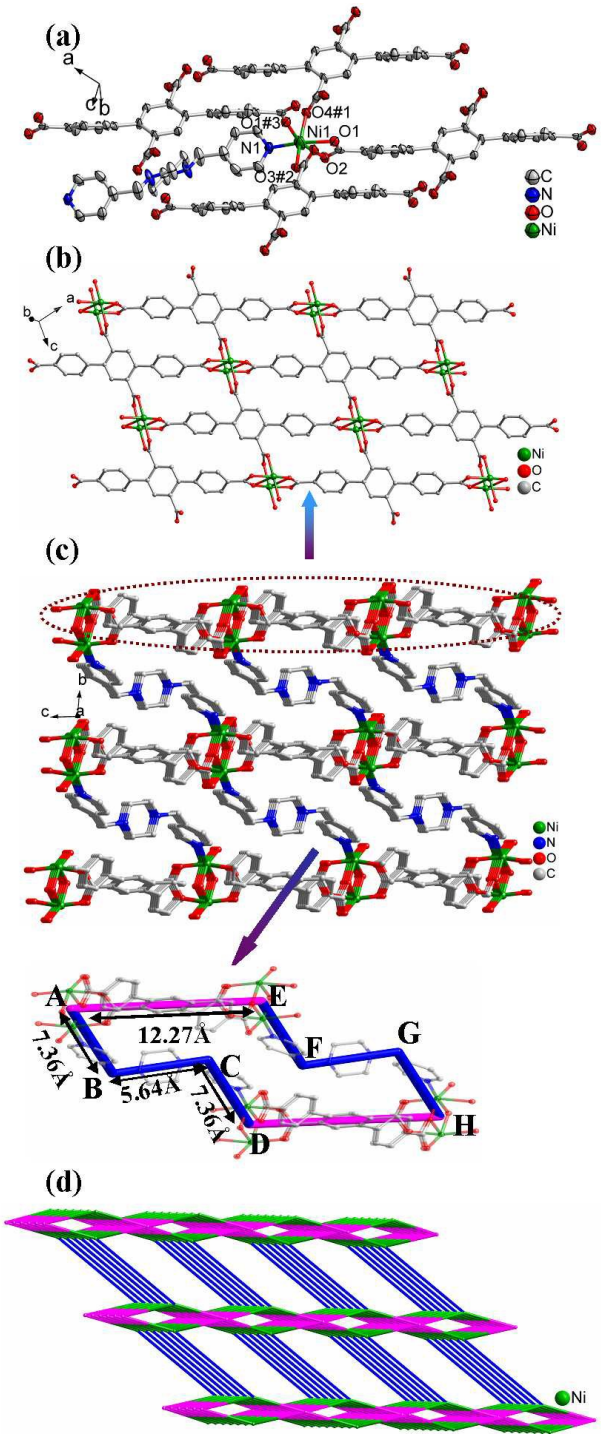

Fig. 5. (a) The coordination environment of the Ni^{II} ion in complex **5** (#1 – 1 + *x*, *y*, *z*; #2 3 – *x*, 1 – *y*, 1 – *z*; #3 2 – *x*, 1 – *y*, 1 – *z*). (b) The 2D layer containing metal Ni^{II} ions and **L** ligands in **5**. (c) The 3D framework with the symmetrical polygonal windows in **5**. (d) The schematic of the 3D framework.

P-1 space group. The asymmetric unit includes one crystallographically independent NiII ion, a half **L** ligand lying about an inversion centre and one half of a **bpmp** ligand lying about another independent inversion centre. The metal Ni^{II}

ion is completed with two chelating oxygen atoms (O1, O2) of one **L** ligand, three bridging oxygen atoms (O1#3, O3#2, O4#1) of three separate **L** ligands and one nitrogen atom (N1) of **bpmp** ligand, locating in the slightly distorted $\{NiO_5N\}$ octahedral coordination configuration (**Fig. 5a**). The distances of Ni–O and Ni–N are 2.023(6)–2.143(5) Å and 2.034(7) Å, respectively. The **L** ligand takes on two kinds of coordination patterns: the carboxylic groups from two-sided phenyl rings are μ_2-η^1:η^2 patterns (chelate-monodentate), and two carboxylic groups of central phenyl ring are μ_2-η^1:η^1 patterns (bidentate) (**Table 2**). The phenyl rings are parallel on both sides of **L** ligand in complex **5**, and they have a dihedral angle of 47.53º with the central phenyl ring. The four carboxylic groups from four **L** ligands link two Ni^{II} ions to construct a dinuclear Ni^{II} unit with the Ni···Ni distance of 2.79 Å (**Fig. S6**). Each μ_8-bridging **L** ligand is linked by the dinuclear Ni^{II} units to form a 2D layer, in which the dinuclear units and the central phenyl rings of **L** ligands divide into the same quadrilaterals with the size of 12.27 Å × 8.95 Å (**Fig. 5b and Fig. S6**). The neighbouring 2D layers are connected by chair-like **bpmp** ligand with the parallel bis-pyridine rings to create a 3D framework, which is composed by the symmetrical polygonal windows with different distances of 12.27 Å (AE=DH), 7.36 Å (AB=EF=CD=GH) and 5.64 Å (BC=FG), respectively (**Fig. 5c**).

From topological viewpoint, each Ni^{II} ion coordinating with four **L** ligands and one **bpmp** ligand is regarded as a 5-connected node. The carboxylate **L** ligand linking eight 5-connected Ni^{II} ions is viewed as a 8-connected node. The **bpmp** ligand as a linker connects two metal Ni^{II} ions. The final framework can be generalized as 2-nodal (5, 8)-connected net with the Schläfli symbol of $\{4^{20}\cdot6^8\}\{4^6\cdot6^4\}_2$ (**Fig. 5d**).

*$\{[Cd(\mathbf{H_2L})(\mathbf{bpe})_{0.5}(H_2O)_2]\cdot0.5(\mathbf{bpe})\}_n$ (**6**)*

Different from the above supramolecular structures, the structural analysis shows that complex **6** is 3D supramolecular framework based on the 2D coordination layers and the non-coordinated **bpe** ligands, crystallizing P-1 space group of triclinic system with the asymmetric unit consisting of one crystallographically independent Cd^{II} ion, two half $\mathbf{H_2L}$ ligands lying about independent inversion centres, two half **bpe** ligands lying about other independent inversion centres, two coordinated water molecules. The metal Cd^{II} ion features a seven-coordinated $\{CdO_6N\}$ pentagonal-bipyramid style, which is lighted by four carboxylic oxygen atoms (O1, O2, O3, O4) from two separate $\mathbf{H_2L}$ ligands, two coordinated water molecules (O9, O10) and one pyridine nitrogen atom (N1) from the **bpe** ligand (**Fig. 6a**). The distances of Cd–O and Cd–N are in the range of 2.317(9)–2.427(8) Å and 2.398(7) Å, respectively. Two carboxylic groups from the central phenyl ring chelate the metal Cd^{II} ion (μ_1-η^1:η^1 coordination mode) (**Table 2**), respectively, producing the wave-type 1D chain, in which two parallel phenyl rings have the dihedral angle of 53.49º with the central phenyl ring. Although the **bpe** ligands display non-coordinated and bidentate coordination fashion, the dihedral angle of the two pyridine rings is 0º. The μ_2-bridging N-donor **bpe** ligands connect the adjacent 1D Cd-$\mathbf{H_2L}$ chains to create the 3-connected 2D $\{6^3\}$ sheet with hexagonal grids containing different distances between the metal Cd^{II} ions (**Fig. 6b**).

The final 3D supramolecular architecture is constructed through the O–H···N hydrogen bonding interactions between the coordinated water molecules (O10) from the 2D structures and the

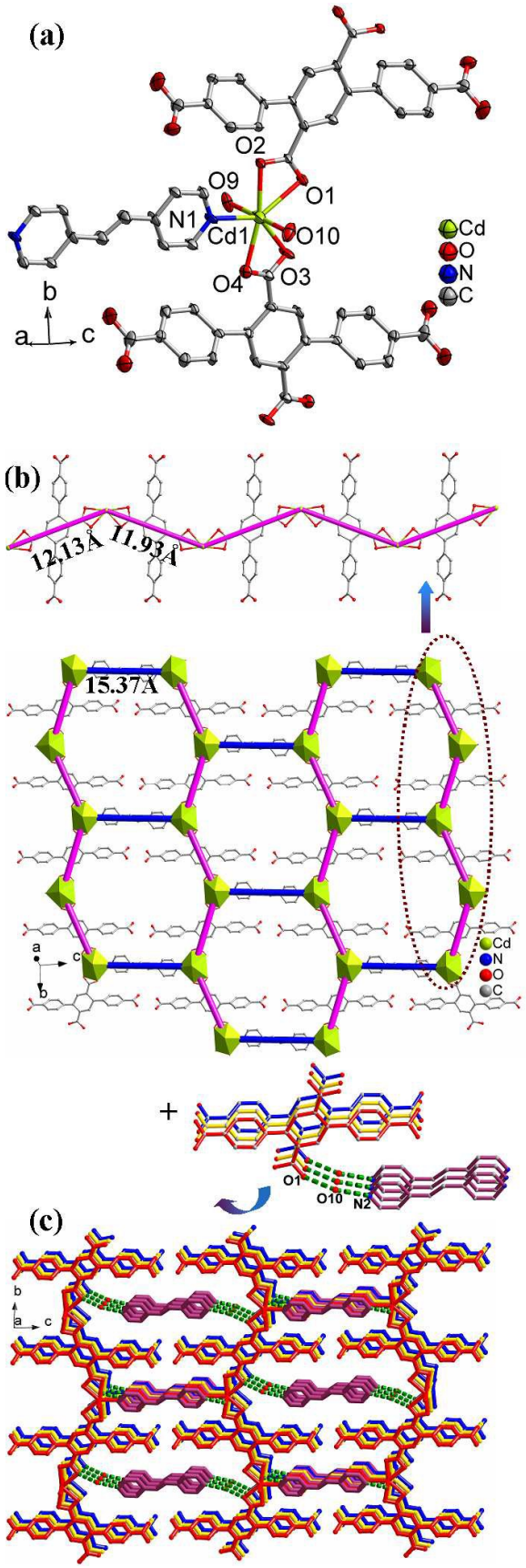

Fig. 6. (a) The coordination environment of the Cd^{II} ion in complex **6**. (b) The 2D layer with hexagonal grids in **6**. (c) View of 3D supramolecular framework formed by hydrogen-bonding interactions in **6**.

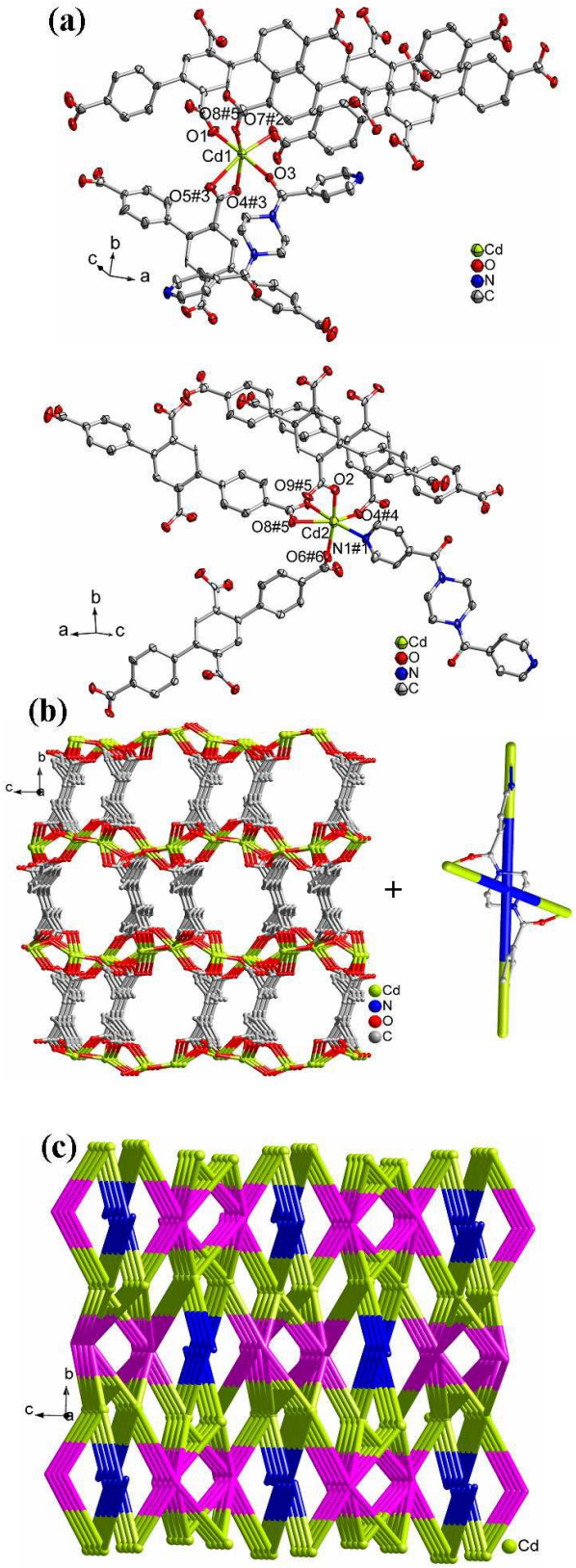

Fig. 7. (a) The coordination environment of the Cd^{II} ion in complex **7** (#1 – 1 + *x*, *y*, *z*; #2 1 + *x*, *y*, *z*; #3 – 1 – *x*, – 1/2 + *y*, –3/2 – *z*; #4 – 1 – *x*, – *y*, – 1 – *z*; #5 – *x*, – *y*, – 1– *z*; #6 1 + *x*, – 1/2 – *y*, 1/2 + *z*). (b) 3D framework based on metal Cd^{II} ions and **L** ligands in **7**. (c) The schematic of the (4,5,5,8)-connected 3D framework with $\{4^{15}\cdot6^{13}\}_2\{4^2\cdot6^3\cdot8\}\{4^7\cdot6^3\}_4$ topology.

nitrogen atoms (N2) from non-coordinated **bpe** ligands with the distance of 2.9899 Å. It is noted that the non-coordinated **bpe** ligands play an important role in sustaining the whole 3D supramolecular framework (**Fig. 6c**).

*{[Cd_2(**L**)(**bpfp**)$_{0.5}$]·H_2O}$_n$ (7)*

In complex **7**, the **bpe** ligand was replaced by the **bpfp** ligand, producing a 3D framework which crystallizes in monoclinic system P2(1)/n space group. In the asymmetric unit, there are two crystallographically independent Cd^{II} ions, one **L** ligand, one half of a **bpfp** ligand lying about an inversion centre and one lattice water molecule. Both six-coordinated Cd^{II} ions represent different coordination environment (**Fig. 7a**). Cd1 is encircled by six oxygen atoms (O1, O3, O4#3, O5#3, O7#2, O8#5) of four separate **L** ligands and carbonyl group of one **bpfp** ligand, which sits distorted {CdO_6} octahedral geometry, while Cd2 is furnished by five oxygen atoms (O2, O4#4, O6#6, O8#5, O9#5) from four separate **L** ligands and one nitrogen atom (N1#1) from one **bpfp**ligand, adopting distorted {CdO_5N} octahedral coordination sphere. The distances of Cd–O and Cd–N are in the range of 2.198(10)–2.486(9) Å and 2.316(12) Å, respectively. For **L** ligand, all the phenyl rings are not parallel: the dihedral angle between two side phenyl rings is 15.97º, and they have the dihedral angles of 61.00º and 46.05º with the central phenyl ring, respectively. The completely deprotonated **L** ligands feature μ_2-η^1:η^1 (bidentate) and μ_2-η^1:η^2 (chelate-monodentate) coordination fashions (**Table 2**), which are coordinated with eight metal Cd^{II} ions to give a 3D skeleton. Different from **3**, four potential coordination atoms (two nitrogen atoms of the parallel pyridine rings and the carbonyl oxygen atoms) from **bpfp** ligand of complex **7** all coordinate with the metal Cd^{II} ions to connect the Cd-**L** 3D skeleton (**Fig. 7b**).

From topological viewpoint, Cd1 and Cd2 are 5-connected by four **L** ligands and one **bpfp** ligand with vertex symbol of $\{4^7\cdot6^3\}$. The **L** ligand linking eight metal Cd^{II} ions is classified as 8-connected node with vertex symbol of $\{4^{15}\cdot6^{13}\}$. The **bpfp** ligand coordinating with four metal Cd^{II} ions is regarded as 4-connected node with vertex symbol of $\{4^2\cdot6^3\cdot8\}$. Thus, the whole 3D architecture can be demonstrated as (4,5,5,8)-connected framework with the Schläfli symbol of $\{4^{15}\cdot6^{13}\}_2\{4^2\cdot6^3\cdot8\}\{4^7\cdot6^3\}_4$ (**Fig. 7c**).

Influence of the differently flexible bis-pyridyl ligands on the architectures of complexes 1–7

In our work, the [1,1′:4′,1″-terphenyl]-2′,4,4″,5′-tetracarboxylic acid (**H_4L**) as the main ligand reacts with the transition metal ions (Co^{II}, Ni^{II} and Cd^{II}) and dissimilarly flexible organic bis-pyridyl ligands (**bpe**, **bpmp** and **bpfp**) to obtain a series of 2D and 3D coordination polymers. Our investigate reveals that the flexibility of the auxiliary bis-pyridyl ligands is very important to construct the different architectures.

In three kinds of bis-pyridyl ligands, comparatively speaking, the **bpe** tends to be the rigid ligand because of the existence of the C=C bonds. The **bpmp** includes not only the flexible piperazidine

ring but also its bilateral –CH_2– backbones, which can be regarded as a flexible ligand. The **bpfp** ligand is similar with the **bpmp** ligand except that the carbonyl groups replace two –CH_2– groups of **bpmp** ligand, enhancing the rigidity of the whole organic ligand. Thus, the flexibility of **bpe**, **bpfp** and **bpmp** increases in turn. Through the structural comparison of the title complexes, it can be clearly seen that the bis-pyridyl ligands play a major role in the coordination modes of $\mathbf{H_4L}$ ligands and formation of the final structures in the same metal-$\mathbf{H_4L}$ system. In complexes **1**–**3**, the partially deprotonated $\mathbf{H_2L}$ ligands exhibit bis(bidentate) coordination mode for **1** and bis(monodentate) coordination mode for **3**, while the fully deprotonated **L** ligand of **2** presents multi-coordination modes. In the ultimate structures, complex **1** is a 2D coordination layer constructed by Co^{II} ions and $\mathbf{H_2L}$ carboxylates, and the **bpe** as the monodentate ligands hang both sides. Complex **2** is a 3D $\{4^3\cdot6^3\}_2\{4^6\cdot6^6\cdot8^3\}$ framework based on the 2D Co-**L** layers and the bidentate **bpmp** ligands, and complex **3** is a (4, 4) 2D sheet. The **bpfp** ligand from **3** falling in between the rigid **bpe** and flexible **bpmp** ligands restricts the deprotonation of $\mathbf{H_2L}$ ligands, and some potential coordinated sites are non-coordinated. For complexes **4** and **5**, the $\mathbf{H_2L}$ with bis(monodentate) coordination mode from **4** are linked by the Ni^{II} ions and the bridging **bpe** ligands to form the 2D grid. In complex **5**, all the oxygen atoms of **L** coordinate with the metal Ni^{II} ions, which are linked through the bridging **bpmp** ligands to build a (5,8)-connected 3D framework. For complexes **6** and **7**, the bis-chelating $\mathbf{H_2L}$ in **6** are connected with the Cd^{II} ions and the bridging **bpe** ligands to construct the hexagonal 2D grid. Different from complex **3**, in complex **7**, all the potential coordinate sites from **L** and **bpfp** ligands coordinate with the metal Cd^{II} ions to form a 3D $\{4^{15}\cdot6^{13}\}_2\{4^2\cdot6^3\cdot8\}\{4^7\cdot6^3\}_4$ framework.

To the best of our knowledge, the literature about the [1,1′:4′,1″-terphenyl]-2′,4,4″,5′-tetracarboxylic acid is very limited. So far only Wang's group has obtained a 3D reticular framework [Cd(**L**)$_{0.5}$(**bipy**)] (**8**) based on the co-ligands (**L** and 2,2′-bipyridine (**bipy**)). This reported complex **8** is different from complexes **6**–**7** in this paper, which may be due to the following reasons: on one hand, the synthetic methods have effect on the construction. Complex **8** was synthesized by the solvothermal method, while complexes **6**–**7** were prepared in the hydrothermal conditions. Though the solvent molecules in complex **8** are absence in the whole framework, they may play the oriented action in the formation of the final 3D skeleton. On the other hand, the selection of the secondary ligands leads to diversely dimensional networks. Owing to the flexibility and the abundant coordinate sites of **bpfp** ligand, it is obvious that complex **7** displays a complicated 3D framework. For the **bpe** ligand of complex **6**, although the flexibility is a little stronger than that of **bipy**, the size is larger than that of **bipy**, which may increase the steric effect in the process of self-assembly in a way.

Powder X-ray diffraction analyses

In order to prove the purities for complexes **1**–**7**, the simulated and experimental powder X-ray diffraction (PXRD) peaks are shown in **Fig. S8**. The experimental patterns correlate with the simulated patterns, which suggest the synthesized samples have the good crystalline purities. The slight differences from the simulated and experimental peaks in intensities may ascribe the preferred orientation of crystals.

Thermogravimetric analyses

To examine the thermal stabilities for complexes **1**–**7**, the thermogravimetric (TG) analyses were explored in flowing nitrogen atmosphere between 30 °C and 800 °C with the heating rate of 10 °C min^{-1}. Complexes **1**–**4** and **6** show two weight loss steps, while complexes **5** and **7** exhibit only one weight loss step (**Fig. S9**). For complex **1**, two weight loss processes of 91.88% happen in the temperature range of 295–650 °C, which corresponds to the decomposition of $\mathbf{H_2L}$ and **bpe** organic ligands (calc. 90.95%). The residual CoO component is about 8.12% (calc. 9.05%). For complexes **2**–**4** and **6**, the weight losses in the first step are 2.36% for **2**, 4.47% for **3**, 10.16% for **4** and 4.42% for **6**, respectively, which may be due to the loss of coordinated water molecules and/or lattice water molecules (calc. 2.23% for **2**, 4.52% for **3**, 10.04% for **4** and 4.90% for **6**). The second weight losses of 79.41% for **2**, 86.64% for **3**, 80.95% for **4** and 80.51% for **6** are shown in the temperature range of 270–590 °C for **2**, 185–750 °C for **3**, 90–600 °C for **4** and 280–600 °C for **6**, arising from the collapse of the organic ligands (calc. 79.19% for **2**, 86.06% for **3**, 79.55% for **4** and 79.80% for **6**). The final products correspond to metal oxide. For complex **5**, only one weight loss of 82.28% is attributed to the decomposition of the organic ligands (calc. 81.04%) from 30 °C to 650 °C, and the residue is NiO of 17.72% (calc. 18.96%). Different from complex **5**, one weight loss of complex **7** is about 72.01% (calc. 71.66%) between 30 °C and 530 °C, indicating the loss of the lattice water molecules and the decomposition of the organic ligands. The remaining product of 27.99% may be due to CdO (calc. 28.34%).

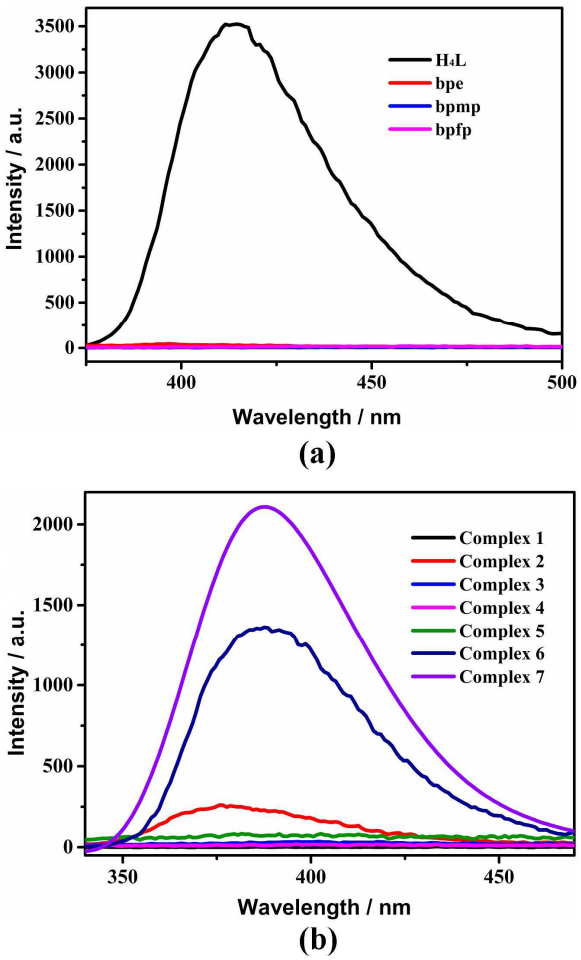

Fig. 8. (a) The solid-state fluorescence spectra of the free ligands **H_4L**, **bpe**, **bpmp** and **bpfp** at room temperature. (b) The solid-state fluorescence spectra of complexes **1**–**7** at room temperature.

Fluorescent properties

Lots of coordination polymers with d^{10} metals as the photosensitive materials have been explored in the field of photochemistry [13]. The solid state fluorescence properties of complexes **1–7** and the free organic ligands (**H_4L**, **bpe**, **bpmp** and **bpfp**) have been examined at the room temperature. In order to make comparisons, all the measurements are carried out under the same test condition. The excitations of the title complexes and the organic ligands are at 280 nm with the excitation slit and emission slit of 1.0 nm. The **H_4L** ligand shows intense emission peaks with the maxima at 413 nm, however, the N-donor ligands (**bpe**, **bpmp** and **bpfp**) have no significant fluorescent emission (**Fig. 8**). As shown in **Fig. 8**, complexes **2**, **6** and **7** exhibit the emission broad peaks at 376 nm, 387 nm and 387 nm, respectively, which present blue shift compared to the **H_4L** ligand. The emergence of these phenomena may be attributed to ligand-to-metal charge transfer, intraligand and metal-to-ligand charge transfer [14]. However, complexes **1**, **3–5** have no fluorescent emission. By comparing the fluorescence properties of complexes **1–7**, the fluorescent intensities of Cd^{II} coordination polymers are greatly higher than those of Co^{II} or Ni^{II} coordination polymers. In virtue of the existence of d−d electron transitions and vibrations of single electrons, the emission of Co/Ni complexes generates obvious quenching [14b]. While Cd^{II} ion possesses core-like d-orbits, and there is no d–d transition [14b], thus complexes **6–7** display strong fluorescence emission.

Electrochemical behaviors of 1–5–CPEs

To study the redox properties of Co^{II} and Ni^{II} complexes, the electrochemical behaviors of complexes **1–5** bulk-modified carbon paste electrodes (**1**–CPE, **2**–CPE, **3**–CPE, **4**–CPE and **5**–CPE) are researched in 0.01 M H_2SO_4 + 0.5 M Na_2SO_4 aqueous solution because of the insolubility in water and the common organic solvents for complexes **1–5**. In **Fig. 9** and **Fig. S10**, the cyclic voltammograms of **1**–CPE, **2**–CPE, **3**–CPE, **4**–CPE and **5**–CPE at different scan rates are investigated in the diverse potential range –100 to 900 mV for **1**–CPE, 100 to 700 mV for **2**–CPE, 50 to 800 mV for **3**–CPE, 100 to 800 mV for **4**–CPE and 200 to 650 mV for **5**–CPE. One pair of reversible redox peak appear at the modified CPEs, which may be due to the redox of Co^{III}/Co^{II} or Ni^{III}/Ni^{II} [15]. The mean peak potentials [$E_{1/2}$ = (E_{pa} + E_{pc})/2] are 410 mV for **1**–CPE, 434 mV for **2**–CPE, 450 mV for **3**–CPE, 429 mV for **4**–CPE and 436 mV for **5**–CPE with the scan rate of 100 mVs^{-1}, respectively (**Fig. S11**). **1**–CPE as an example is researched the effect of scan rates on the electrochemical property. The peak potentials shift gradually with the increased scan rate from 25 to 500 mVs^{-1}: the cathodic peak potentials shifted to negative direction and the corresponding anodic peak potentials shifted to positive direction. As shown in the insert of **Fig. 9**, the redox peak currents are proportional to the scan rates, which reveal that the redox of **1**–CPE is the surface-confined process.

Photocatalytic activities

Organic dyes as the high soluble environmental pollutants are hard to be degraded through conventional techniques. Photocatalytic degradation as a kind of effective way can decompose organic dyes to be CO_2 and the small organic acids. According to the

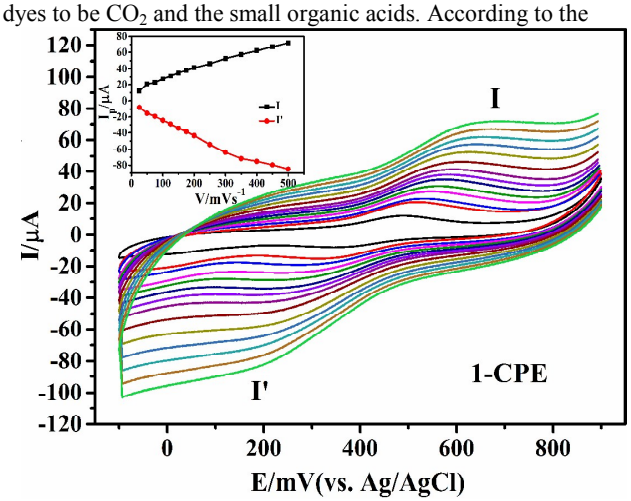

Fig. 9. Cyclic voltammograms of the **1**–CPE in 0.01 M H_2SO_4 + 0.5 M Na_2SO_4 aqueous solution at different scan rates (from inner to outer: 25, 50, 75, 100, 125, 150, 175, 200, 250, 300, 350, 400, 450, 500 $mV{\cdot}s^{-1}$). The inset shows the plots of the anodic and cathodic peak currents against scan rates.

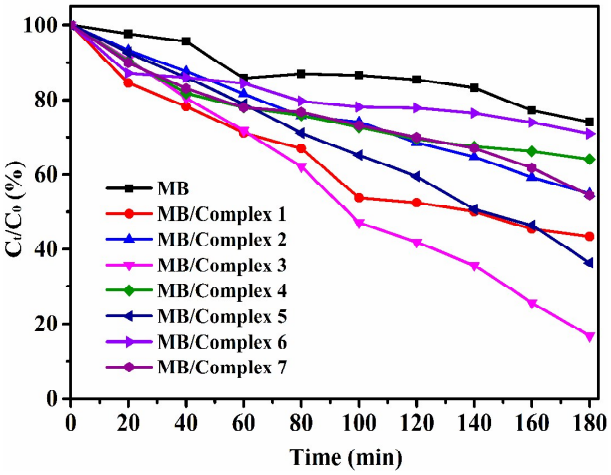

Fig. 10. Photocatalytic decomposition rates of MB solution under the visible light irradiation with the use of the title complexes and no crystal in the same conditions.

literatures, some coordination polymers possess excellent photocatalytic effect in the course of degrading organic dyes [5]. Herein, we chose methylene blue (MB) as the model of dye pollutant, and we investigated the photocatalytic properties of complexes **1–7** to the degradation of MB under visible light irradiation.

For the photocatalytic degradation of complexes **1–7**, the visible light induces three kinds of N-containing ligands and the carboxylate ligand to bring nitrogen and/or oxygen-metal charge transfer, enhancing electrons from the highest occupied molecular orbital (HOMO) to the lowest unoccupied molecular orbital (LUMO). The HOMO needs one electron to go back to its stable state, so the electron was caught from water molecules, which was oxygenated to produce the ·OH radicals [16]. Then MB may be decomposed through ·OH active species effectively, which complete the photocatalytic process [16a,17].

The photocatalytic experiments were carry out in the typical processes, 100 mg samples were dispersed in 10.0 mg /L MB aqueous solution 200 mL, stirred in the dark for 30 min magnetically to achieve the adsorption/desorption equilibrium. Subsequently, the mixture was irradiated under visible light of a 300W xenon lamp, kept stirring. 3 mL suspension was taken out from the reactor every 20 min, which was handled through centrifugal separation. Then they were analyzed by UV-visible spectroscopy. Moreover, the comparative experiment of MB without any photocatalyst has also been performed in the same conditions.

There is no obvious change in the degradation of MB without any catalyst by the visible light irradiation (**Fig. S13a**). However, when complexes **1–7** act as the photocatalysts, the absorption intensities of MB decreased gradually with longer illumination time. In **Fig. 10**, the concentrations of MB (C) versus irradiation times (t) for the title complexes are plotted. The degradations increase from about 25.2% (without any catalyst) to 56.6% for **1**, 45.0% for **2**, 83.2% for **3**, 35.9% for **4**, 63.6% for **5**, 29.1% for **6** and 45.5% for **7** after 180 min. Complexes **1–5** and **7** display the photocatalytic activities in the degradation of MB (**Fig. S13b–e, g** and **Fig. 11**). While the degradation of complex **6** close to that of MB without any catalyst, so complex **6** should be no degradation effect (**Fig. S13f**). In addition, the control experiments of the title reactants ($Co(NO_3)_2·6H_2O$, $Ni(NO_3)_2·6H_2O$, $CdCl_2·2.5H_2O$, H_4L, **bpe**, **bpmp** and **bpfp**) have been investigated, and there is no significant change for the degradation of MB. The phenomena reveal that complex **3** shows good photocatalytic activity **Fig. 11**, which may be the potential photoactive materials for degradation of some dyes.

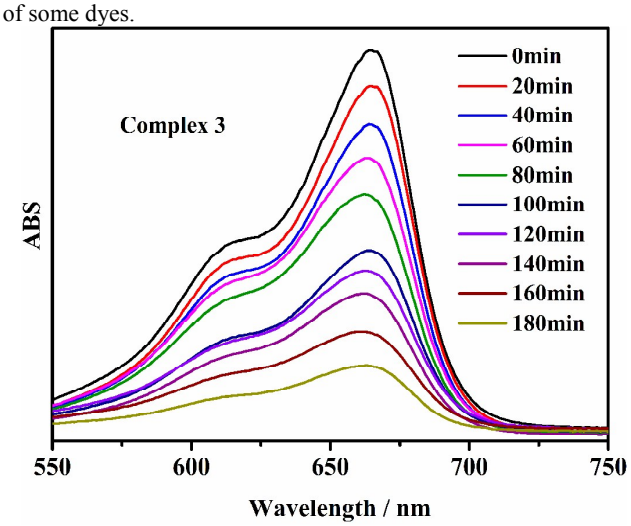

Fig. 11. Absorption spectra of the MB solution during the decomposition reaction under the visible light irradiation with the presence of complex **3**.

After the photocatalytic experiments, PXRD patterns of complexes **1–7** were measured again. **Fig. S8** shows that the PXRD peaks are almost identical to that of the fresh complexes, proving the stabilities of the title complexes.

The photocatalytic behaviours of the title complexes for the degradation of organic dyes MB have been researched. In addition, the solid UV-vis spetra of the title complexes have been measured (**Fig. S12**). Through theoretical calculation of band gaps form complexes **1–7**, the band gap value of complex **3** is the lowest, which may lead to the good photocatalytic activity compared with the other complexes. From the perspective of structure, different complexes display different catalytic activities owing to the coordination conjugation of the metal ions, the selection of organic ligands and the differences of the final complexes. To our knowledge, the photocatalytic properties of coordination polymers based on the tetracarboxylate ligands with terphenyl moiety have no report so far.

Conclusion

In conclusion, the simple one-pot hydrothermal system was investigated to prepare a series of diversely structural coordination polymers derived from the main ligands [1,1′:4′,1″-terphenyl]-2′,4,4″,5′-tetracarboxylic acid (H_4L) and three kinds of auxiliary bis-pyridyl ligands. The different flexibilities from the bis-pyridyl ligands have the significant influence on the structural diversities of the title complexes. The electrochemical behaviors of complexes **1–5** have been studied. Fluorescent properties display that complexes **6–7** based on d^{10} metals exhibit the strong fluorescent intensities compared with complexes **1–5** in the same condition, revealing that they might be candidates in the fluorescent field. In addition, complex **3** possesses good photocatalytic activity for degradation of MB, which may be the

potential photoactive material.

Acknowledgement

This work was supported by the Program for National Nature Science Foundation of China (nos. 21271024 and 20971014) and Beijing Natural Science (no. 2112037).

Notes and references

1 (a) J. R. Li, J. Sculley and H. C. Zhou, *Chem. Rev.*, 2012, **112**, 869; (b) L. E. Kreno, K. Leong, O. K. Farha, M. Allendorf, R. P. Van Duyne and J. T. Hupp, *Chem. Rev.*, 2012, **112**, 1105; (c) M. Hirscher, *Angew. Chem. Int. Ed.*, 2011, **50**, 581; (d) J. P. Zhang, Y. B. Zhang, J. B. Lin and X. M. Chen, *Chem. Rev.*, 2012, **112**, 1001; (e) Z. C. Hu, B. J. Deibert and J. Li, *Chem. Soc. Rev.*, 2014, **43**, 5815; (f) X. Zhao, X. H. Bu, Q. G. Zhai, H. Tran and P. Y. Feng, *J. Am. Chem. Soc.*, 2015, **137**, 1396; (g) C. B. He, K. D. Lu and W. B. Lin, *J. Am. Chem. Soc.*, 2014, **136**, 12253; (h) H. L. Jiang and Q. Xu, *Chem. Commun.*, 2011, **47**, 3351; (i) R. Vaidhyanathan, S. S. Iremonger, G. K. H. Shimizu, P. G. Boyd, S. Alavi and T. K. Woo, *Science*, 2010, **330**, 650.

2 (a) P. P. Zhang, J. Peng, H. J. Pang, J. Q. Sha, M. Zhu, D. D. Wang, M. G. Liu and Z. M. Su, *Cryst. Growth Des.*, 2011, **11**, 2736; (b) J. M. R. Narayanam and C. R. J. Stephenson, *Chem. Soc. Rev.*, 2011, **40**, 102; (c) C. Tian, Q. Zhang, A. Wu, M. Jiang, Z. Liang, B. Jiang and H. Fu, *Chem. Commun.*, 2012, **48**, 2858.

3 (a) A. Fujishima, X. Zhang and D. A. Tryk, *Surf. Sci. Rep.*, 2008, **63**, 515; (b) A. Kar, Y. R. Smith and V. Subramanian, *Environ. Sci. Technol.*, 2009, **43**, 3260; (c) H. X. Li, X. Y. Zhang, Y. N. Huo and J. Zhu, *Environ. Sci. Technol.*, 2007, **41**, 4410; (d) Z. L. Liao, G. D. Li, M. H. Bi and J. S. Chen, *Inorg. Chem.*, 2008, **47**, 11.

4 (a) Y. Q. Chen, S. J. Liu, Y. W. Li, G. R. Li, K. H. He, Y. K. Qu, T. L. Hu and X. H. Bu, *Cryst. Growth Des.*, 2012, **12**, 5426; (b) L. L. Wen, J. B. Zhao, K. L. Lv, Y. H. Wu, K. J. Deng, X. K. Leng and D. F. Li, *Cryst. Growth Des.*, 2012, **12**, 1603; (c) J. Guo, J. Yang, Y. Y. Liu and J. F. Ma, *CrystEngComm*, 2012, **14**, 6609.

5 (a) X. L. Wang, J. Luan, F. F. Sui, H. Y. Lin, G. C. Liu and C. Xu, *Cryst. Growth Des.*, 2013, **13**, 3561; (b) X. L. Wang, F. F. Sui, H. Y. Lin, J. W. Zhang and G. C. Liu, *Cryst. Growth Des.*, 2014, **14**, 3438; (c) X. L. Wang, J. J. Huang, L. L. Liu, G. C. Liu, H. Y. Lin, J. W. Zhang, N. L. Chen and Y. Qu, *CrystEngComm*, 2013, **15**, 1960; (d) X. L. Wang, X. T. Sha, G. C. Liu, N. L. Chen and Y. Tian, *CrystEngComm*, 2015, **17**, 7290; (e) H. H. Wang, J. Yang, Y. Y. Liu, S. Y. Song and J. F. Ma, *Cryst. Growth Des.*, 2015, **15**, 4986; (f) M. Li, S. Zhao, Y. F. Peng, B. L. Li and H. Y. Lia, *Dalton Trans.*, 2013, **42**, 9771.

6 (a) M. J. Katz, J. E. Mondloch, R. K. Totten, J. K. Park, S. T. Nguyen, O. K. Farha and J. T. Hupp, *Angew. Chem., Int. Ed.*, 2014, **53**, 497; (b) A. A. Talin, A. Centrone, A. C. Ford, M. E. Foster, V. Stavila, P. Haney, R. A. Kinney, V. Szalai, F. El Gabaly, H. P. Yoon, F. Léonard and M. D. Allendorf, *Science*, 2014, **343**, 66; (c) L. Sun, C. H. Hendon, M. A. Minier, A. Walsh and M. Dinca, *J. Am. Chem. Soc.*, 2015, **137**, 6164; (d) D. Sheberla, L. Sun, M. A. Blood-Forsythe, S. Er, C. R. Wade, C. K. Brozek, A. Aspuru-Guzik and M. Dinca, *J. Am. Chem. Soc.*, 2014, **136**, 8859.

7 (a) J. G. Duan, B. S. Zheng, J. F. Bai, Q. A. Zhang and C. Y. Zuo, *Inorg. Chim. Acta*, 2010, **363**, 3172; (b) B. Zheng, J. F. Bai and Z. X. Zhang, *CrystEngComm*, 2010, **12**, 49; (c) J. F. Eubank, F. Nouar, R. Luebke, A. J. Cairns, L. Wojtas, M. Alkordi, T. Bousquet, M. R. Hight, J. Eckert, J. P. Embs, P. A. Georgiev and M. Eddaoudi, *Angew. Chem. Int. Ed.*, 2012, **51**, 10099; (d) V. Guillerm, Ł. J. Weseliński, Y. Belmabkhout, A. J. Cairns, V. D'Elia, Ł. Wojtas, K. Adil and M. Eddaoudi, *Nat. Chem.*, 2014, **6**, 673.

8 (a) A. Y. Robin and K. M. Fromm, *Coord. Chem. Rev.*, 2006, **250**, 2127; (b) M. J. Sie, Y. J. Chang, P. W. Cheng, P. T. Kuo, C. W. Yeh, C. F. Cheng, J. D. Chen and J. C. Wang, *CrystEngComm*, 2012, **14**, 5505.

9 (a) W. Y. Gao, W. M. Yan, R. Cai, K. Williams, A. Salas, L. Wojtas, X. D. Shi and S. Q. Ma, *Chem. Commun.*, 2012, **48**, 8898; (b) C. Y. Wang, Z. M. Wilseck and R. L. LaDuca, *Inorg. Chem.*, 2011, **50**, 8997; (c) L. Luo, P. Wang, G. C. Xu, Q. Liu, K. Chen, Y. Lu, Y. Zhao and W. Y. Sun, *Cryst. Growth Des.*, 2012, **12**, 2634.

10 (a) X. T. Zhang, L. M. Fan, X. Zhao, D. Sun, D. C. Li and J. M. Dou, *CrystEngComm*, 2012, **14**, 2053; (b) L. M. Fan, X. T. Zhang, W. Zhang, Y. S. Ding, W. L. Fan, L. M. Sun, Y. Pang and X. Zhao, *Dalton Trans*., 2014, **43**, 6701; (c) X. Zhou, P. Liu, W. H. Huang, M. Kang, Y. Y. Wang and Q. Z. Shi, *CrystEngComm*, 2013, **15**, 8125; (d) Y. L. Wu, G. P. Yang, Y. Q. Zhao, W. P. Wu, B. Liu and Y. Y. Wang, *Dalton Trans.*, 2015, **44**, 3271; (e) X. Lin, I. Telepeni, A. J. Blake, A. Dailly, C. M. Brown, J. M. Simmons, M. Zoppi, G. S. Walker, K. M. Thomas, T. J. Mays, P. Hubberstey, N. R. Champness and M. Schröder, *J. Am. Chem. Soc*., 2009, **131**, 2159; (f) X. Lin, J. H. Jia, X. B. Zhao, K. M. Thomas, A. J. Blake, G. S. Walker, N. R. Champness, P. Hubberstey and M. Schröder, *Angew. Chem., Int. Ed*., 2006, **45**, 7358.

11 (a) X. T. Zhang, L. M. Fan, Z. Sun, W. Zhang, D. C. Li, P. H. Wei, B. Li and J. M. Dou, *J. Coord. Chem*., 2012, **65**, 3205; (b) L. M. Fan, X. T. Zhang, Z. Sun, W. Zhang, D. C. Li, P. H. Wei, B. Li and J. M. Dou, *J. Coord. Chem*., 2012, **65**, 4389; (c) Y. L. Gai, F. L. Jiang, L. Chen, Y. Bu, K. Z. Su, S. A. Al-Thabaiti and M. C. Hong, *Inorg. Chem*., 2013, **52**, 7658; (d) Y. L. Wu, G. P. Yang, X. Zhou, J. Li, Y. Ning and Y. Y. Wang, *Dalton Trans.*, 2015, **44**, 10385; (e) B. B. Kang, N. Wei and Z. B. Han, *RSC Adv.*, 2015, **5**, 1605.

12 (a) G. M. Sheldrick, *Acta Crystallogr., Sect. A: Found. Crystallogr.*, 2008, **64**, 112; (b) L. J. Bourhis, O. V. Dolomanov, R. J. Gildea, J. A. K. Howard and H. Puschmann, *Acta Cryst.* 2015, **A71**, 59; (c) O. V. Dolomanov, L. J. Bourhis, R. J. Gildea, J. A. K. Howard and H. Puschmann, *J. Appl. Cryst.* 2009, **42**, 339.

13 (a) M. D. Allendorf, C. A. Bauer, R. K. Bhaktaa and R. J. T. Houka, *Chem. Soc. Rev.*, 2009, **38**, 1330; (b) X. Q. Yao, M. D. Zhang, J. S. Hu, Y. Z. Li, Z. J. Guo and H. G. Zheng, *Cryst. Growth Des.*, 2011, **11**, 3039.

14 (a) Y. J. Cui, Y. F. Yue, G. D. Qian and B. L. Chen, *Chem. Rev.*, 2012, **112**, 1126; (b) H. Y. Li, L. H. Cao, Y. L. Wei, H. Xu and S. Q. Zang, *CrystEngComm*, 2015, **17**, 6297.

15 T. V. Mitkina, N. F. Zakharchuk, D. Y. Naumov, O. A. Gerasko, D. Fenske and V. P. Fedin, *Inorg. Chem.*, 2008, **47**, 6748.

16 (a) H. X. Yang, T. F. Liu, M. N. Cao, H. F. Li, S. Y. Gao and R. Cao, *Chem. Commun.*, 2010, **46**, 2429; (b) Y. Q. Chen, S. J. Liu, Y. W. Li, G. R. Li, K. H. He, Y. K. Qu, T. L. Hu and X. H. Bu, *Cryst. Growth Des.*, 2012, **12**, 5426.

17 (a) J. X. Meng, Y. Lu, Y. G. Li, H. Fu and E. B. Wang, *CrystEngComm*, 2011, **13**, 2479; (b) J. Guo, J. Yang, Y. Y. Liu and J. F. Ma, *CrystEngComm*, 2012, **14**, 6609.

A series of coordination polymers tuned terphenyl tetracarboxylates and bipyridyl ligands with different flexibilities manifesting fluorescence properties and photocatalytic activities

Bao Mu, Ru-dan Huang*

Key Laboratory of Cluster Science of Ministry of Education, School of Chemistry, Beijing Institute of Technology, Beijing, 100081, P. R. China

Seven new coordination polymers derived from terphenyl tetracarboxylates and bipyridyl ligands with different flexibilities have been successfully prepared under hydrothermal conditions. The effect of the bipyridyl ligands with different flexibilities on the architectures of complexes **1**–**7** have been investigated in detail. The electrochemical behaviors of complexes **1**–**5**, fluorescence and photocatalytic properties of complexes **1**–**10** have also been studied.

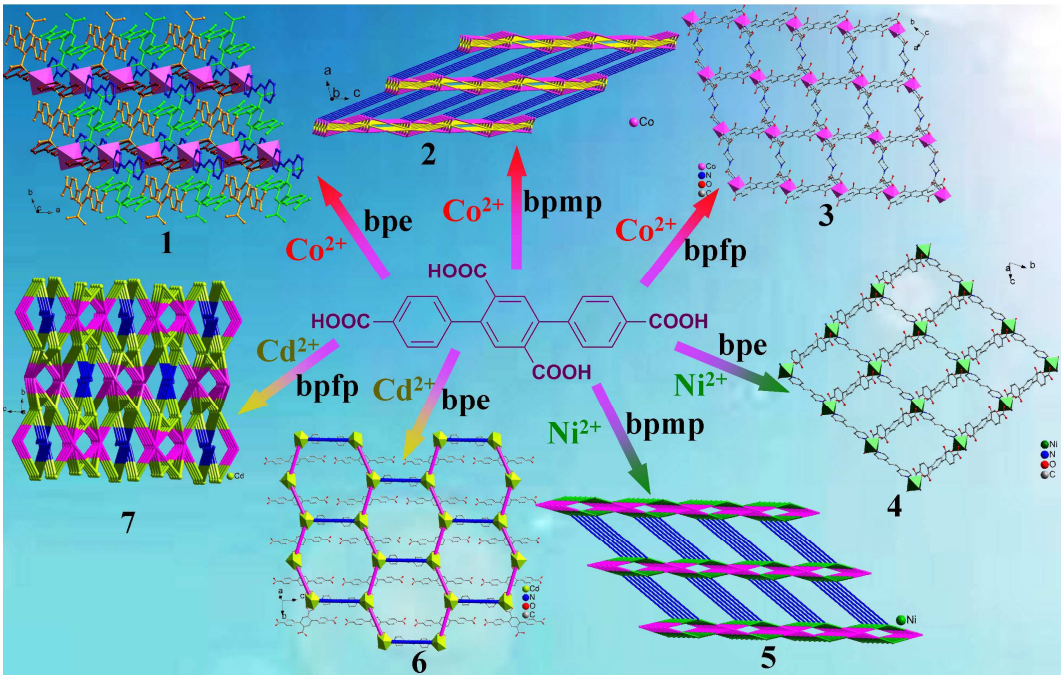

* Corresponding author. *E-mail address:* huangrd@bit.edu.cn (R. D. Huang).